Analyst

RSC Publishing

PAPER

View Article Online
View Journal | View Issue

Cite this: *Analyst*, 2013, **138**, 4040

Aberration-free FTIR spectroscopic imaging of live cells in microfluidic devices

K. L. Andrew Chan† and Sergei G. Kazarian*

The label-free, non-destructive chemical analysis offered by FTIR spectroscopic imaging is a very attractive and potentially powerful tool for studies of live biological cells. FTIR imaging of live cells is a challenging task, due to the fact that cells are cultured in an aqueous environment. While the synchrotron facility has proven to be a valuable tool for FTIR microspectroscopic studies of single live cells, we have demonstrated that high quality infrared spectra of single live cells using an ordinary Globar source can also be obtained by adding a pair of lenses to a common transmission liquid cell. The lenses, when placed on the transmission cell window, form pseudo hemispheres which removes the refraction of light and hence improve the imaging and spectral quality of the obtained data. This study demonstrates that infrared spectra of single live cells can be obtained without the focus shifting effect at different wavenumbers, caused by the chromatic aberration. Spectra of the single cells have confirmed that the measured spectral region remains in focus across the whole range, while spectra of the single cells measured without the lenses have shown some erroneous features as a result of the shift of focus. It has also been demonstrated that the addition of lenses can be applied to the imaging of cells in microfabricated devices. We have shown that it was not possible to obtain a focused image of an isolated cell in a droplet of DPBS in oil unless the lenses are applied. The use of the approach described herein allows for well focused images of single cells in DPBS droplets to be obtained.

Received 15th February 2013
Accepted 12th March 2013

DOI: 10.1039/c3an00327b

www.rsc.org/analyst

Introduction

There is an urgent need for label-free methods for the analysis of live biological cells. Such methods could provide insights into cell differentiation, ageing and other processes within the cells, such as the response to chemotherapeutic drugs, which is important for improving the understanding and prevention of disease. FTIR spectroscopic imaging of live cells may be one of the methods of choice. However, its use in transmission has been a difficult task and much of the recent research in this area has focused on overcoming some of the challenges of such measurements.[1] One of the major obstacles is that water absorbs strongly in the mid-IR region, particularly in the O–H stretch region between 3700 and 2900 cm^{-1} and the OH bending region at around 1640 cm^{-1}. Live cells are maintained in aqueous environments, as such their measurement in transmission mode requires very small path lengths ($\sim$10 μm) in order to preserve the integrity of the spectral regions of interest. The use of a synchrotron source for FTIR microscopy has proven to be a powerful method for measuring live cells.[2–9] The high brightness of the synchrotron allows a small, diffraction limited, aperture size to be used while at the same time obtaining spectra with high signal to noise ratios. The high signal to noise ratio allows the absorbance of other components of live cells to be revealed after the subtraction of water. However, when access to beamline at synchrotron facilities is not possible, the development of live cell measurements using an ordinary IR source is required. Challenges related to the presence of water and spatial resolution were addressed by imaging live cells in attenuated total internal reflection (ATR) mode using a removable objective with germanium crystal.[10] The IR light in an ATR spectroscopic measurement probes up to a few micrometers into the live cell, which is approximately the thickness of a spread cell, thereby effectively avoiding the absorption from the bulk medium above the living cells. Micro ATR imaging also has the advantage of enhanced spatial resolution due to the increase in numerical aperture through the high refractive index ATR element.[11–13] Other advantages of ATR imaging have been discussed in our previous study[14] and recent applications of ATR FTIR imaging to cells and tissues have been summarized in a very recent review.[15] However, due to the small path length of ATR (not more than a few micrometers), the spectra obtained often are of somewhat lower signal to noise ratios when compared to measurements made in transmission mode.

Measurement of live cells in an aqueous environment usually involves the use of liquid sample cell where the live cells

Department of Chemical Engineering, Imperial College London, SW7 2AZ, London, UK. E-mail: s.kazarian@imperial.ac.uk; Tel: +44 (0)207 5945574

† Current address: Kings College London, Institute of Pharmaceutical Science, London, UK.

in medium, are sandwiched between two infrared transparent windows.[8,16–19] A material commonly used as the window is CaF_2 due to its low solubility in water and ability to support the growth of a number of cell lines.[9] However, when imaging is carried out through thick CaF_2 windows, chromatic aberration becomes a serious issue.[8,20,21] This effect has recently been investigated by Tobin *et al.* who reported a reduction in chromatic aberration when using a thin CaF_2 window.[22] In another work, a sub-micrometer thick diamond window was introduced to reduce chromatic as well as spherical aberrations while studying living biological samples in a flow chamber.[23] In order to remove the effect of refraction, we have adapted a lens that is made of the same material as the window (CaF_2) of the transmission liquid cell.[24] When the lens is placed on top of the window, a pseudo hemisphere is formed on the sample such that the infrared light, which is typically, collected through an inverse Cassegrain infrared microscope objective, leaves the higher refractive index CaF_2 surface into air at the normal angle to the CaF_2/air interface. Note that the centre thickness and the radius of the curvature of the lens were chosen such that sum of the centre thickness of the lens and the thickness of the window will be the same as the radius of the curvature of the lens (*i.e.* to form a hemisphere on the sample as shown in Fig. 1c). As a result of using the lens, the IR light does not disperse or refract and therefore produces no chromatic or spherical aberration. We have previously demonstrated that chromatic aberration is the dominating obfuscation in FTIR imaging, caused by differing depths of focus across the spectral range,[24] therefore we will be focusing our discussion on the effect and removal of chromatic aberration. While the main advantage of using this lens is the removal of aberrations, the lens also acts as a solid immersion lens which increases magnification and the spatial resolution of the system by increasing the numerical aperture, as has previously been demonstrated in the visible region.[25] As a result, the magnification and the spatial resolution are improved by the value of the refractive index of the material which, in this case, is ~1.4.

In our previous work,[24] only one lens was used such that the optics on the objective side did not match with the optics on the condenser side. As a result, a lower throughput of light, hence a lower signal to noise ratio, was observed but it was still sufficient for obtaining FTIR images of tissues and polymeric samples. In this study of imaging of live cells, two lenses are employed such that samples are effectively sandwiched between two pseudo hemispheres (as shown in Fig. 1c). This improved approach has now been applied to the study of live cells in microfluidic devices.

Microfluidics for live cell studies has certain advantages over closed liquid cell chambers such as reduced shear stress on the cells during sample insertion or closing and sealing of the optical windows as well as providing the ability to easily change the medium.[1] There are a number of strategies to create the microfabricated devices for cell studies including using photoresists or lithographic patterning[17,22,26] and open channel microfluidics.[27] The potential of combining microfluidic devices with FTIR imaging has been introduced previously.[28] In this work, we applied a wax print directly onto the surface of the infrared windows in a microfluidic flow cell, an approach that was introduced in our previous studies,[29,30] to create various new devices (Fig. 1b) and combined this with the

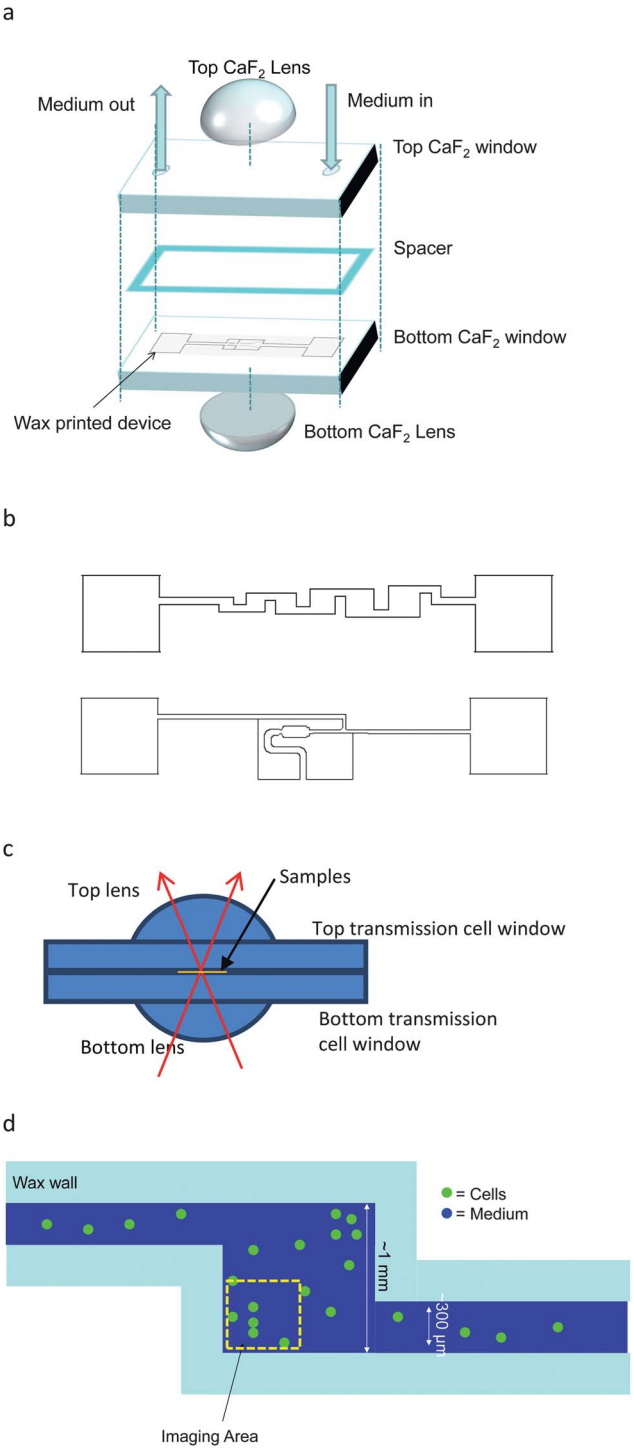

Fig. 1 (a) Schematic diagram showing the liquid cell and the two lenses used in this experiment. (b) Some of the designs of the microfabricated device used in this study. The top design was used for imaging the cells in medium (DMEM), the bottom design was used for imaging cells in DPBS droplets in oil. (c) Schematic diagram showing the two lenses (one on top and one on the bottom) attached to the transmission cell windows such that the infrared light passes through the system without significant refraction. (d) Schematics of the cells in microfluidic device (a zoom in diagram of the top device shown in (b)).

lenses to obtain effectively aberration free FTIR images of live cells.

Experimental

FTIR images were measured with a continuous scan spectrometer (IFS 66, Bruker Optics, Germany) combined with an infrared microscope (IRscopeII, Bruker Optics, Germany) equipped with a focal plane array detector (64 × 64 or 128 × 128) and a visible camera. The microscope consists of a set of reflective optics including a 15× inverse Cassegrain condenser and objective with a numerical aperture of 0.4. The visible camera and the FPA detector in the microscope were aligned such that in normal transmission imaging measurements without the use of a CaF_2 window on top of the sample, sharp images can be obtained in both visible and IR modes. Spectra were measured across the spectral range 3940 cm^{-1} to 1000 cm^{-1}, 200 scans and 8 cm^{-1} spectral resolution. All spectra (4096 or 16 384) were measured simultaneously. Integrated absorbance was used for plotting the absorbance of specific spectral bands for the construction of the corresponding chemical images. Obtaining an image in this study typically took 5–8 minutes depending on the number of pixels used. Such acquisition times were required to produce spectra with sufficiently high signal to noise ratios.

Infrared transparent liquid cells with 12 μm (or 25 μm spacers for the droplet flow measurement) (Omin cell, Specac Ltd, UK) were used in these experiments (Fig. 1a). The sample cell consists of two CaF_2 windows and the thickness of both windows is 4 mm. The microfabricated (or microfluidic) device was created by first printing the design on the surface of one of the CaF_2 windows by the mean of wax printing. The design was made using Microsoft Paint software and translated into a Macro code using in-house software which could be directly read and printed onto the 4 mm CaF_2 window using the microdroplet system (AutoDrop®, Microdrop, Germany). Some of the designs of the device are shown in Fig. 1b. Polywax™ 500 (mp 88 °C, Sigma-Aldrich) was used as the "ink" of the printer and the channel walls of the device were made of these wax droplets. The diameter of each wax droplet was ~50 μm. Further details on this method of microfabrication of fluid channels can be found elsewhere.[27] A holder was used to clamp the windows together with screws (not shown in Fig. 1a) with the spacer and the printed device sandwiched in between the windows such that the designed channels were sealed.

A CaF_2 lens with a diameter of 10 mm, a radius of the curvature of 10 mm and a center thickness of 6 mm (Crystran Ltd, UK) was aligned on top of the 4 mm thick CaF_2 window such that a pseudo hemisphere was formed. Further details for the setup of the top lens were explained in a previous work,[24] the second lens (which was not used in the approach described previously) was placed on the bottom side of the window to form a pseudo hemisphere in a similar manner as the lens on top. This is done by first securing the bottom lens on the microscope stage on an o-ring, supported by modeling clay, such that the flat surface of the lens is parallel to the microscope stage. The liquid cell was then placed on top of the lens such that the flat surface of the lens is in contact with the bottom window of the liquid cell. The main function of the bottom lens is to improve the throughput of light of the system.

Human embryonic kidney (HEK 293) cell-line was cultured in Dulbecco's modified Eagle's medium (DMEM, pH ~ 7.4, Invitrogen) with 10% foetal calf serum (Invitrogen) at 5% CO_2 and 37 °C. Cells were harvested using 0.25% trypsin EDTA when ~70% confluence was reached. The cell suspension was then centrifuged into a pellet followed by re-suspension in ~8 ml of medium (DMEM) giving a cell concentration of ~1×10^6 per ml. ~0.2 ml of the cell suspension was then injected into the microfabricated device with a 1 ml syringe until a number of cells appeared in the device. The syringe was then removed and the remaining cell suspension discarded. The syringe was then refilled with medium (DMEM) that had been equilibrated in air with 5% CO_2. A constant flow of the equilibrated medium was then applied to the device at a flow rate of 80 nl min^{-1} using a syringe pump (Pump 11 Elite, Harvard Apparatus Ltd). The liquid cell was then placed on a heater such that the temperature of the liquid cell reached ~37 °C. The cells were incubated in this condition for 24 hours before FTIR images were taken.

For the cells in the aqueous (Dulbecco's Phosphate-Buffered Saline, DPBS, pH ~ 7.4, Sigma-Aldrich) droplet in oil experiment, the cells were harvested as described above. The cell pellet was then rinsed with 1 ml of DPBS 3× and then re-suspended in DPBS (1 ml) giving a cell concentration of ~1×10^7 per ml. The cell suspension was injected from into the left entrance of the microfluidic device at a flow rate of 0.1 μl min^{-1} while oil (FC40, Sigma Aldrich) was injected through the right channel at a flow rate of 0.5 μl min^{-1} using the syringe pumps.

Results and discussion

The design of the microfabricated device was made in an attempt to create regions of the channel where flow was slower such that cells would settle in those areas (see schematic diagram in Fig. 1d). It was found that the cells did settle in the corner areas as expected. The flow of the fresh medium was maintained at ~80 nl min^{-1} such that there was a constant supply of nutrient to the cells in the closed device.

Imaging live cells without lens

The live cells in the microfabricated device were first imaged without the lens and the resultant images are shown in Fig. 2. The cell image was first focused and captured using visible light (see Fig. 2a) which was followed immediately by FTIR imaging (Fig. 2b and c). Since the image was focused in the visible region, the measurement made in the infrared region was out of focus as a result of the chromatic aberration which can be observed in Fig. 2b and c. These results also demonstrate that the chromatic aberration is clearly worse when the longer wavelengths of light are used to generate the image *i.e.* those that are further away from the focusing wavelengths. FTIR images were generated by plotting the values of the integrated area under the selected band with straight baselines as a 2-D map. Fig. 2b shows that it is just about possible to capture the

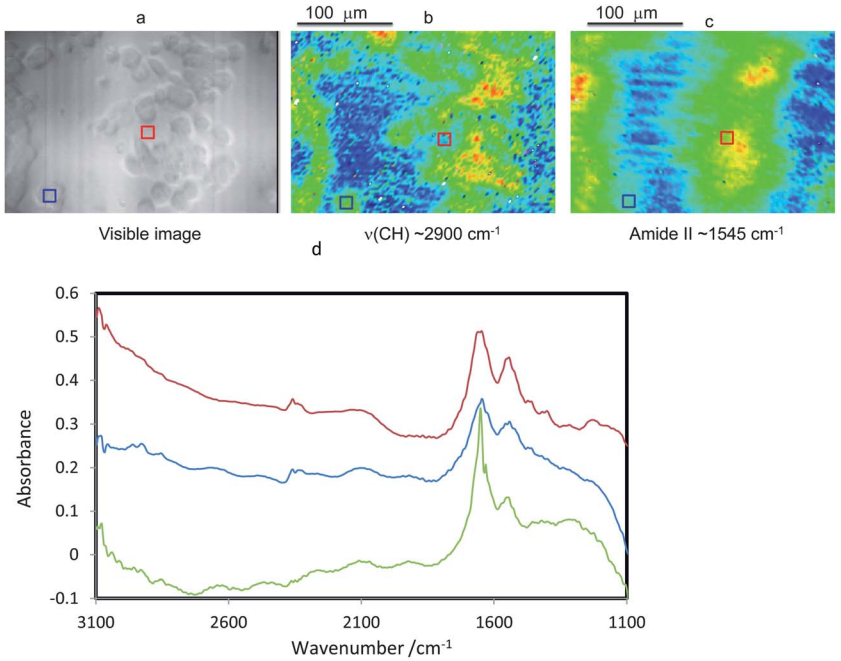

Fig. 2 Images measured without lens added on top of the transmission cell. (a) Visible image, (b) FTIR image based on ν(CH) and (c) FTIR image based on the amide II band of the proteins in live cells in the microfabricated device. (d) Averaged extracted spectra from image (b) or (c). Red spectrum (top) represents the averaged spectra from the area indicated by the red square in the middle of the images (b) or (c), blue spectrum (middle) represents the averaged spectra from the area indicated by the blue square in the bottom left of the images (b) or (c), green spectrum (bottom) represents a single spectrum extracted from within the blue square.

outline of the cell clusters using the ν(C–H) band (baseline across 3000–2800 cm^{-1}) while Fig. 2c shows that the image generated using the amide II band (baseline across 1580–1500 cm^{-1}) is completely out of focus. Apart from the reduced sharpness, and hence spatial resolution, of the images due to the shift of focus, spectra extracted from these images were also affected. To demonstrate this, two averaged spectra were extracted from areas indicated on Fig. 2b and c by the red squares (each square contains 9 spectra). The contribution from water was subtracted to reveal the protein and lipid bands of the cells. The averaged spectrum from the blue square on the bottom left of the images in Fig. 2a–c is shown by the blue line in Fig. 2d, which presents the IR absorbance from an isolated single cell. The spectrum has a clear ν(C–H) band but the amide III and the $\nu_{as}(PO_2)$ bands in the 1270–1230 cm^{-1} region, which are expected to be present in a cell, appear to be diminished. The averaged spectrum from the red square in the middle of the images in Fig. 2a–c is shown by the red line in Fig. 2d, which measures the IR absorbance from the cell-free area in between two cell clusters. The spectrum, in this case, shows almost negligible ν(C–H) absorbance, which is in better focus, while the amides and the $\nu_{as}(PO_2)$ band, which is in poorer focus, remain prominent. These spectra are erroneous considering that they were extracted from an area containing no cells. A non-averaged spectrum (green line) is also extracted from within the blue square region to demonstrate the quality of the raw data. The effect of chromatic aberration clearly creates inconsistencies in spectral information across the spectral range. This could hamper efforts in multivariate analysis where a large spectral range is examined.

Imaging live cells with lens

To correct the effect of chromatic aberration, two CaF_2 lenses were used. One of the lenses was placed on top of the transmission cell windows directly above the sample, the other one was placed underneath the bottom of the transmission cell windows as shown in Fig. 1c. Visible and FTIR images of the same area have been obtained and are shown in Fig. 3. The cells in the microfabricated device were first brought into focus using visible light (Fig. 3a), which was followed immediately by FTIR imaging. The images shown in Fig. 3b and c were generated using the ν(C–H) band and the amide II band, respectively. FTIR images are generated using the same integration methods as those used in Fig. 2. In contrast to the results obtained without lenses (Fig. 2), all three images are in good focus. The outlines of the cells are more clearly shown (compared to the images obtained without the lenses) both from the image generated using the ν(C–H) band at 2900 cm^{-1} and the image generated using the amide II band at 1545 cm^{-1}. This clearly demonstrates that chromatic aberration has been removed and the chemical images generated using different wavelengths of light remain in sharp focus.

Averaged spectra were extracted from the areas indicated by blue and red squares as shown in Fig. 3b and c. The extracted spectra are shown in Fig. 3d. The spectra were extracted in a similar manner and from the same sample areas as those extracted and shown in Fig. 2. The spectrum extracted from the blue square near the bottom left corner, which measures the IR absorbance from the single cell shows clear ν(C–H), amides and $\nu_{as}(PO_2)$ bands as expected. The extracted spectra are clearly

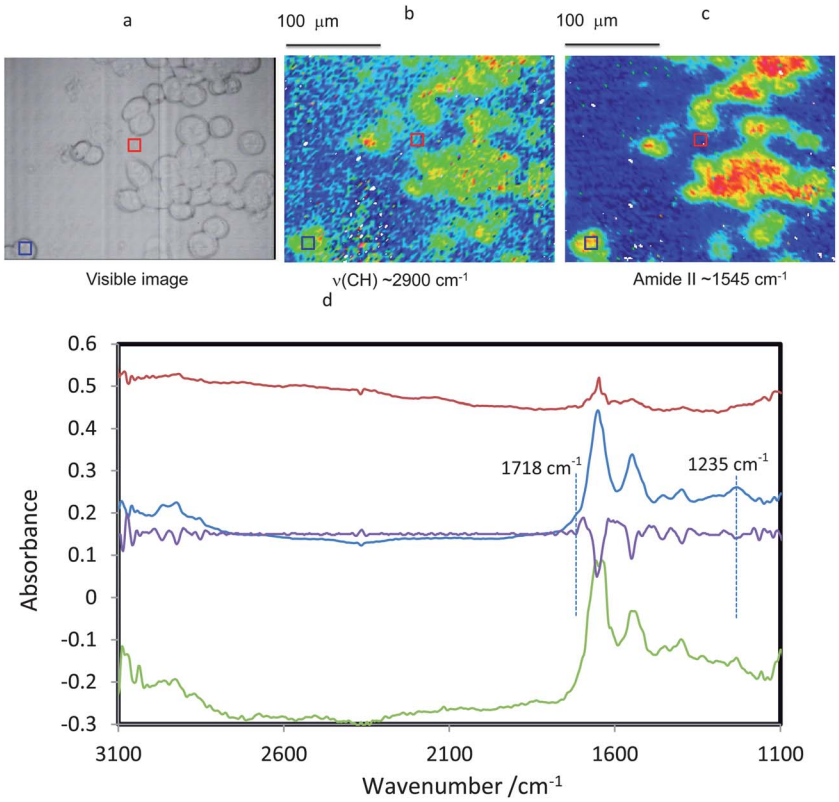

Fig. 3 Images measured with the application of lenses to the transmission cell. (a) Visible image, (b) FTIR image based on ν(CH) and (c) FTIR image based on the amide II band of the proteins in live cells in the microfabricated device. (d) Averaged extracted spectra from image (b) or (c). Red spectrum (top) represents the averaged spectra from the area indicated by the red square in the middle of the images (b) or (c), blue and purple spectra (middle) represent the averaged spectra from the area indicated by the blue square in the bottom left of the images (b) or (c) and the corresponding 2nd derivative, respectively. The green spectrum (bottom) represents a single spectrum extracted from within the blue square.

shown to more accurately represent the sample in the extracted area than the spectra extracted from comparable areas of the image measured without the lens. As a result of the correction of the chromatic aberration, the spectra extracted from the live cell measured with the lenses have a flatter baseline than that extracted from the measurement without the lenses, thus demonstrating added value of the lenses. A second derivative spectrum (purple line) has been calculated from the blue line. The base pair carbonyl from the DNA and RNA at ~1718 cm^{-1} is just about detectable while the $\nu_{as}(PO_2)$ position is located at ~1235 cm^{-1} which indicate the RNA, which is abundant in live cells, is in the "A" conformation.[31] The averaged spectrum extracted from the red square at the middle of the image in Fig. 3, which measures the gap between two cell clusters, shows that all bands are diminished as would be expected in the absence of cells. The spectrum shows a spike in the amide I region because the water δ(O–H) band was not completely subtracted since the absorbance in that region was close to saturation. Apart from that and the ν(O–H) region (which is not shown), most other spectral regions remain accessible. Comparing the spectra of Fig. 2 and 3, it is clear that the spectra measured with the lenses provide a more accurate representation of composition of the area where they were measured. The spectra shown in Fig. 3, especially the one extracted from the single cell on the bottom left corner of the image in Fig. 3b, demonstrate the high signal to noise ratio that may be achieved by this imaging approach. The presented spectrum was an average of 9 spectra which improves the sensitivity of the measurement. The root mean square (RMS) noise level of that spectrum was found to be ~3.8 e^{-4}. It can be seen from images in Fig. 3b and c that the size of a single cell is approximately 20 μm in diameter. The projected size of each pixel is 1.9 μm, therefore it is possible to obtain the averaged spectra from more pixels (*e.g.* 25 spectra from a 5 × 5 square) from a single cell to further improve on the signal to noise ratio when necessary. Note that comparison of the spectra obtained with and without lenses in Fig. 2 and 3 also shows that the absorbance of the libration mode of water in the region (2300–2000 cm^{-1}) is not fully compensated after subtraction of the water contribution because of the effect of chromatic aberration. By contrast, using the lenses ensures uniform subtraction without residual absorbance of water in that region.

With the aid of the lens to improve the imaging and spectral quality, more detailed studies of live cells in a microfluidic device is possible. During the process of incubation, some cells start to attach and spread onto the CaF_2 window. The visible and FTIR images of the cells before and after spreading are shown in Fig. 4a–d. Before spreading, the cells were smaller and the absorbance of the amide II band was stronger. When the cells start to spread, an increase in the area of the cell and a

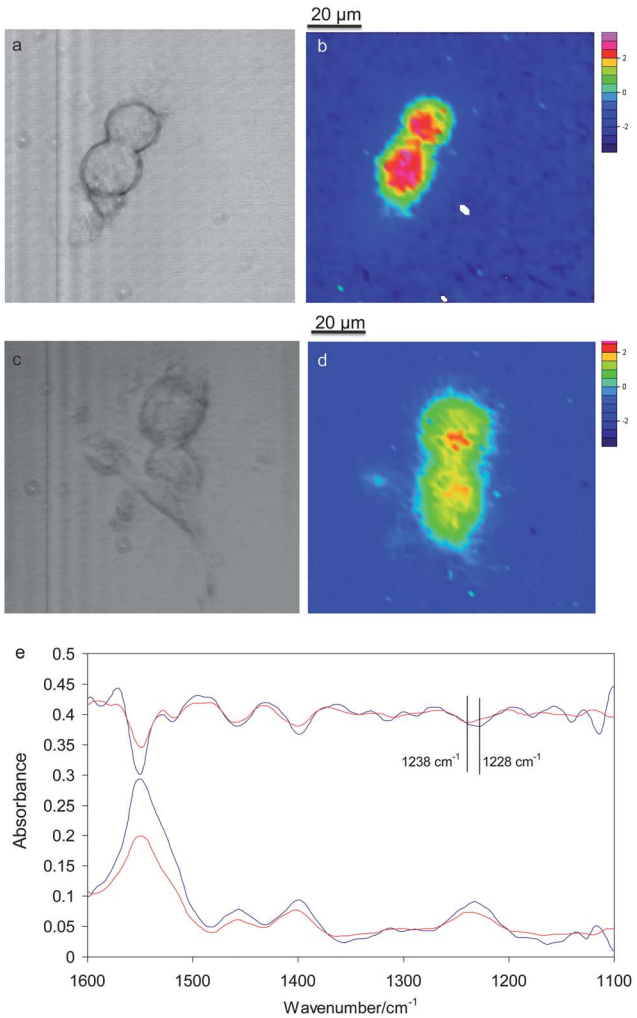

Fig. 4 Visible (a and c) and FTIR (b and d) images (generated using the amide II band at 1545 cm^{-1}) of a few adjacent cells. Images (a) and (b) are captured immediately after injecting the cells into the device, images (c) and (d) are captured after cells have started to spread. (e) Averaged spectra from cells (bottom) and their corresponding 2nd derivatives spectra (top) before (blue lines) and after (red lines) spreading.

drop in the absorbance of the amide II band is observed. This indicates that as the cells spread, they span over a larger area and the cell thickness decreases. Averaged spectra have been extracted from the cells and they are shown in Fig. 4e. The reduction in cell thickness is clearly visible with all the spectral bands that correspond to the cells decreasing as the cells spread. Interestingly the second derivative spectra, taken before and after cell spreading, has indicated a shift of the $\nu_{as}(PO_2)$ band from ~1228 cm^{-1} to ~1238 cm^{-1}. This is indicative of a change in the DNA or RNA conformation during cell spreading.[31] A larger scale of study will be conducted in future to confirm this observation.

Live cells in water droplets in oil

The ability to measure infrared spectra of live cells in aqueous droplets in oil can be a powerful tool for the *in situ* analysis of compartmentalized single cell experiments. We have explored the possibility to capture FTIR images of aqueous droplets in oil where live cells are carried in the aqueous phase (DPBS) and use this to demonstrate the importance of applying the lenses to these types of systems. Cells in a DPBS droplet in oil were created using a microfluidic device containing a T-junction (schematically presented in Fig. 5a). The flow rates of oil and cell suspension in DPBS were adjusted until the flow of cell suspension-in-oil droplets was established. An oil flow rate of 0.5 μl min^{-1} and a cell suspension flow rate of 0.1 μl min^{-1} were found to be suitable values to achieve this flow pattern. Since the imaging time in these experiments was relatively long (minutes) the FTIR images of cells in the DPBS droplet was measured when the flow of oil and cell suspension was stopped to allow the droplets to become stationary. It is possible to capture FTIR images with a millisecond imaging rate[32,33] enabling the measurement of droplets in flow. However, the signal to noise ratio, as a result of the short acquisition time,

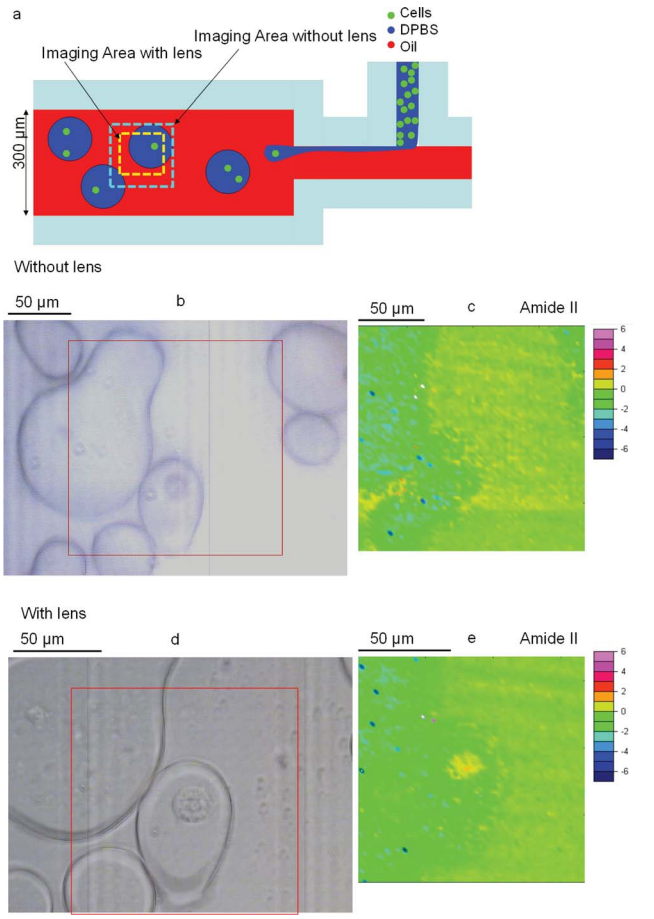

Fig. 5 (a) Schematics of the cells in microfluidic device in droplet flow (a zoom in of the bottom device shown in Fig. 1b). (b) Visible image of a single cell in a DPBS droplet in oil captured without the lenses. The red square shows the area where FTIR image was captured and shown in (c). (c) FTIR image (without the lenses) of the single cell in the DPBS droplet in oil generated using the amide II band. (d) Visible image of same single cell in the DPBS droplet captured with the lenses. The red square shows the area where FTIR image was captured and shown in (e). (e) FTIR image (with the lenses) of the same single cell in the DPBS droplet generated using the amide II band.

will be relatively poor and negatively impact upon the imaging of cells. At this time, it is only possible to measure cells in droplets when the droplet is stationary. On the other hand, it is envisioned that when brighter sources and improved optics are introduced, the imaging of cells in moving droplets may be possible. Here, the visible and corresponding FTIR images of a cell in a droplet, measured without the lenses, are shown in Fig. 5b and c. It was not possible to locate the cells when the lenses were not used because it was not possible to achieve a good focus on the small cells at all wavenumbers when strong chromatic aberration was present. When the lenses were applied the single cell became detectable in the FTIR image (Fig. 5d and e).

Conclusions

This work has demonstrated the removal of the detrimental effect of chromatic aberration on FTIR imaging measurements of live cells through thick CaF_2 windows using the easily adapted approach of adding two lenses. This is particularly important for imaging studies of single live cells as the shifting of focus as a result of the chromatic aberration not only affects the quality of the image but also the quality and reliability of the spectra extracted from different areas of the image. The lenses, when introduced to the transmission windows, form a pseudo sphere over the sample, which significantly reduces the refraction and dispersion of light that causes the chromatic aberration. This allowed us to obtain chemical images that are well focused across different wavelengths of infrared light, which is essential for FTIR spectroscopic imaging of living systems since spectra with broad spectral ranges are measured from different locations simultaneously.

The application of this approach has also been demonstrated for obtaining much sharper images of high spectral quality when imaging live cells in microfabricated and microfluidic systems. The results have demonstrated that it is possible to detect single cells trapped in droplets of DPBS in oil using FTIR spectroscopic imaging when the lens was used. The methodology introduced in this paper allows chemical images of live cells in microfluidic devices to be obtained, which is particularly significant as this was achieved without the recourse to a synchrotron source of infrared radiation. This provides a powerful and noninvasive tool that can facilitate further studies of biochemical processes within live cells using this label-free technique.

Acknowledgements

S. G. K. acknowledges research funding from the European Research Council under the European Community's Seventh Framework Programme (FP7/2007–2013)/ERC advanced grant agreement no. [227950]. We thank Dr Jennifer Dougan and Dr James Kimber for their help and advice.

References

1 L. Quaroni and T. Zlateva, *Analyst*, 2011, **136**, 3219–3232.
2 H. Y. N. Holman, R. Goth-Goldstein, E. A. Blakely, M. C. Martin and W. R. McKinney, *Abstr. Pap. Am. Chem. Soc.*, 2000, **219**, U101.
3 H. Y. N. Holman, K. A. Bjornstad, M. P. McNamara, M. C. Martin, W. R. McKinney and E. A. Blakely, *J. Biomed. Opt.*, 2002, **7**, 417–424.
4 H. Y. N. Holman, M. C. Martin and W. R. McKinney, *Spectroscopy*, 2003, **17**, 139–159.
5 K. L. Goff, L. Quaroni, T. Pedersen and K. E. Wilson, in *Wirms 2009: 5th International Workshop on Infrared Microscopy and Spectroscopy with Accelerator Based Sources*, Amer Inst Physics, Melville, 2009, vol. 1214, pp. 54–56.
6 H. Y. N. Holman, H. A. Bechtel, Z. Hao and M. C. Martin, *Anal. Chem.*, 2010, **82**, 8757–8765.
7 L. Chen, H. Y. N. Holman, Z. Hao, H. A. Bechtel, M. C. Martin, C. B. Wu and S. Chu, *Anal. Chem.*, 2012, **84**, 4118–4125.
8 K. L. Munro, K. R. Bambery, E. A. Carter, L. Puskar, M. J. Tobin, B. R. Wood and C. T. Dillon, *Vib. Spectrosc.*, 2010, **53**, 39–44.
9 D. A. Moss, M. Keese and R. Pepperkok, *Vib. Spectrosc.*, 2005, **38**, 185–191.
10 M. K. Kuimova, K. L. A. Chan and S. G. Kazarian, *Appl. Spectrosc.*, 2009, **63**, 164–171.
11 A. J. Sommer, L. G. Tisinger, C. Marcott and G. M. Story, *Appl. Spectrosc.*, 2001, **55**, 252–256.
12 K. L. A. Chan, S. G. Kazarian, A. Mavraki and D. R. Williams, *Appl. Spectrosc.*, 2005, **59**, 149–155.
13 S. G. Kazarian and K. L. A. Chan, *Appl. Spectrosc.*, 2010, **64**, 135A–152A.
14 K. L. A. Chan and S. G. Kazarian, *Analyst*, 2006, **131**, 126–131.
15 S. G. Kazarian and K. L. A. Chan, *Analyst*, 2013, **138**, 1940–1951.
16 J. R. Mourant, R. R. Gibson, T. M. Johnson, S. Carpenter, K. W. Short, Y. R. Yamada and J. P. Freyer, *Phys. Med. Biol.*, 2003, **48**, 243–257.
17 G. Birarda, G. Grenci, L. Businaro, B. Marmiroli, S. Pacor, F. Piccirilli and L. Vaccari, *Vib. Spectrosc.*, 2010, **53**, 6–11.
18 E. J. Marcsisin, C. M. Uttero, M. Miljkovic and M. Diem, *Analyst*, 2010, **135**, 3227–3232.
19 R. Zhao, L. Quaroni and A. G. Casson, *Analyst*, 2010, **135**, 53–61.
20 G. L. Carr, *Rev. Sci. Instrum.*, 2001, **72**, 1613–1619.
21 D. L. Wetzel, *Vib. Spectrosc.*, 2002, **29**, 291–297.
22 M. J. Tobin, L. Puskar, R. L. Barber, E. C. Harvey, P. Heraud, B. R. Wood, K. R. Bambery, C. T. Dillon and K. L. Munro, *Vib. Spectrosc.*, 2010, **53**, 34–38.
23 M. J. Nasse, S. Ratti, M. Giordano and C. J. Hirschmugl, *Appl. Spectrosc.*, 2009, **63**, 1181–1186.
24 K. L. A. Chan and S. G. Kazarian, *Anal. Chem.*, 2013, **85**, 1029–1036.
25 Q. Wu, L. P. Ghislain and V. B. Elings, *Proc. IEEE*, 2000, **88**, 1491–1498.
26 L. Vaccari, G. Birarda, L. Businaro, S. Pacor and G. Grenci, *Anal. Chem.*, 2012, **84**, 4768–4775.

27 H. Y. N. Holman, R. Miles, Z. Hao, E. Wozei, L. M. Anderson and H. Yang, *Anal. Chem.*, 2009, **81**, 8564–8570.
28 S. G. Kazarian, *Anal. Bioanal. Chem.*, 2007, **388**, 529–532.
29 K. L. A. Chan, X. Z. Niu, A. J. de Mello and S. G. Kazarian, *Lab Chip*, 2010, **10**, 2170–2174.
30 K. L. A. Chan and S. G. Kazarian, *Spectroscopy*, 2012, **27**, 22–27.
31 D. R. Whelan, K. R. Bambery, P. Heraud, M. J. Tobin, M. Diem, D. McNaughton and B. R. Wood, *Nucleic Acids Res.*, 2011, **39**, 5439–5448.
32 K. L. A. Chan, X. Niu, A. J. deMello and S. G. Kazarian, *Anal. Chem.*, 2011, **83**, 3606–3609.
33 K. L. A. Chan and S. G. Kazarian, *Anal. Chem.*, 2012, **84**, 4052–4056.